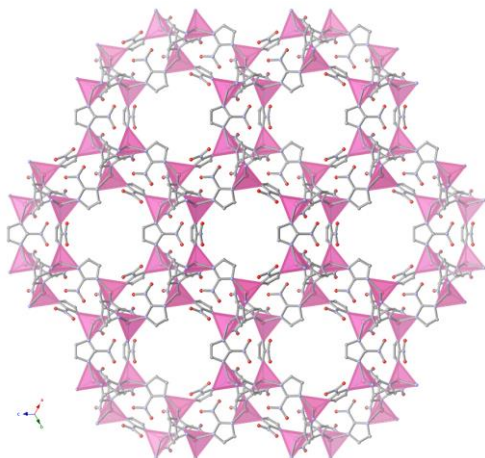
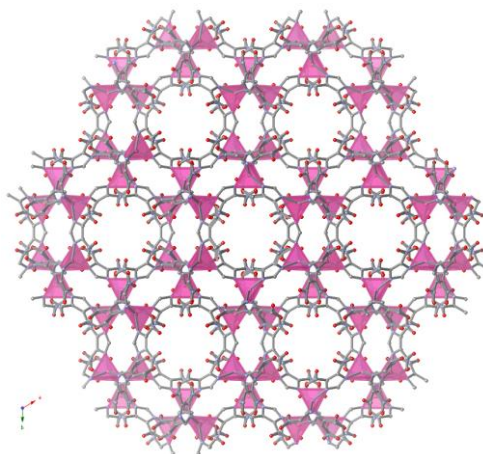
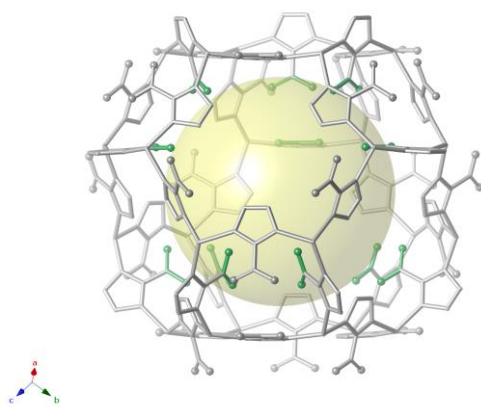
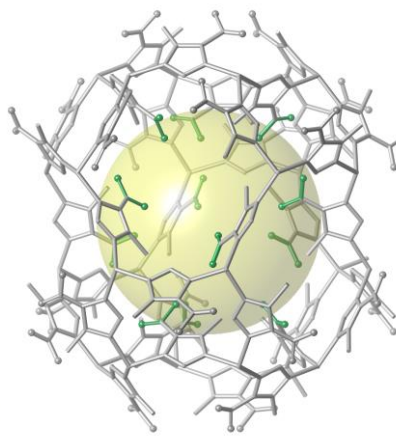
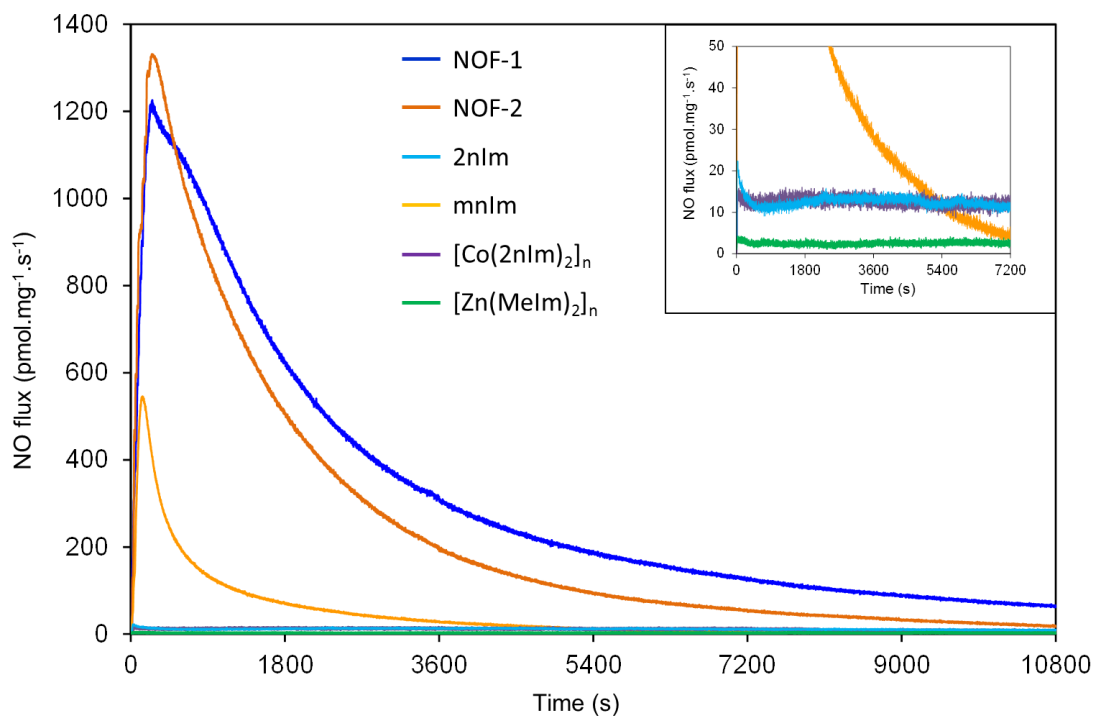


Supplementary Figure S1. FESEM images of NOF-1 and NOF-2. Samples of NOF-1 (a, b, c) and NOF-2 (d, e, f) were obtained by repeatedly spin casting (2000 rpm) methanolic NOF suspensions on 22 x 22 mm glass slides (scale bars: a, b, d, e; 1 μm , c, f; 100 μm). Images c and f show a relatively uniform distribution of the crystals on the glass substrate.

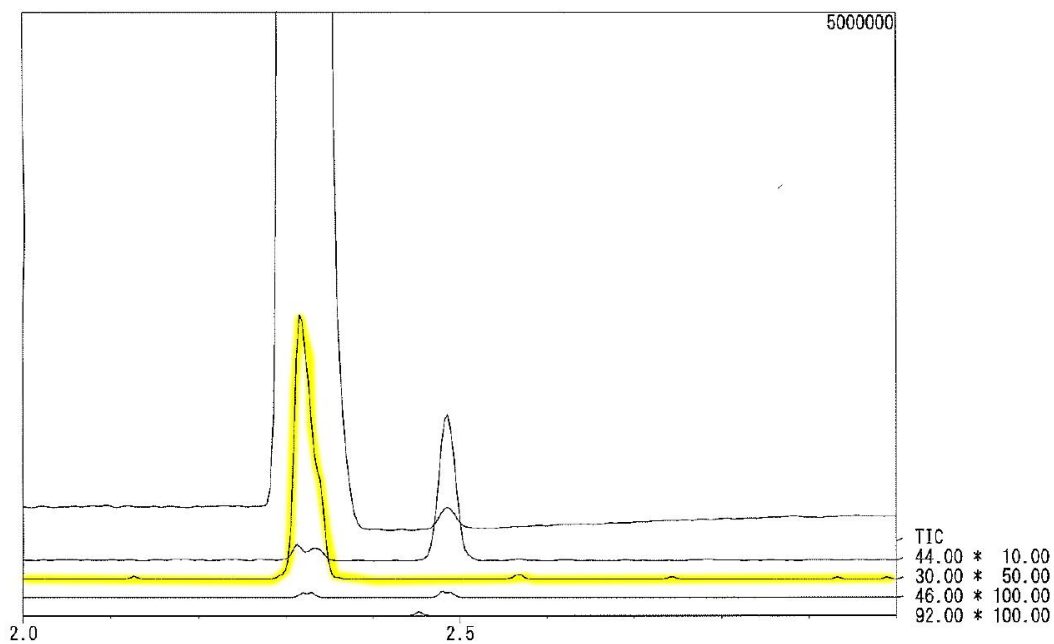
a**b****c****d**

Supplementary Figure S2. Crystallographic representation of NOF-1 (a, c) and NOF-2 (b, d). The sodalite cages represented in c and d highlight the imidazolate ligands which have their nitro groups pointing towards the inner void.

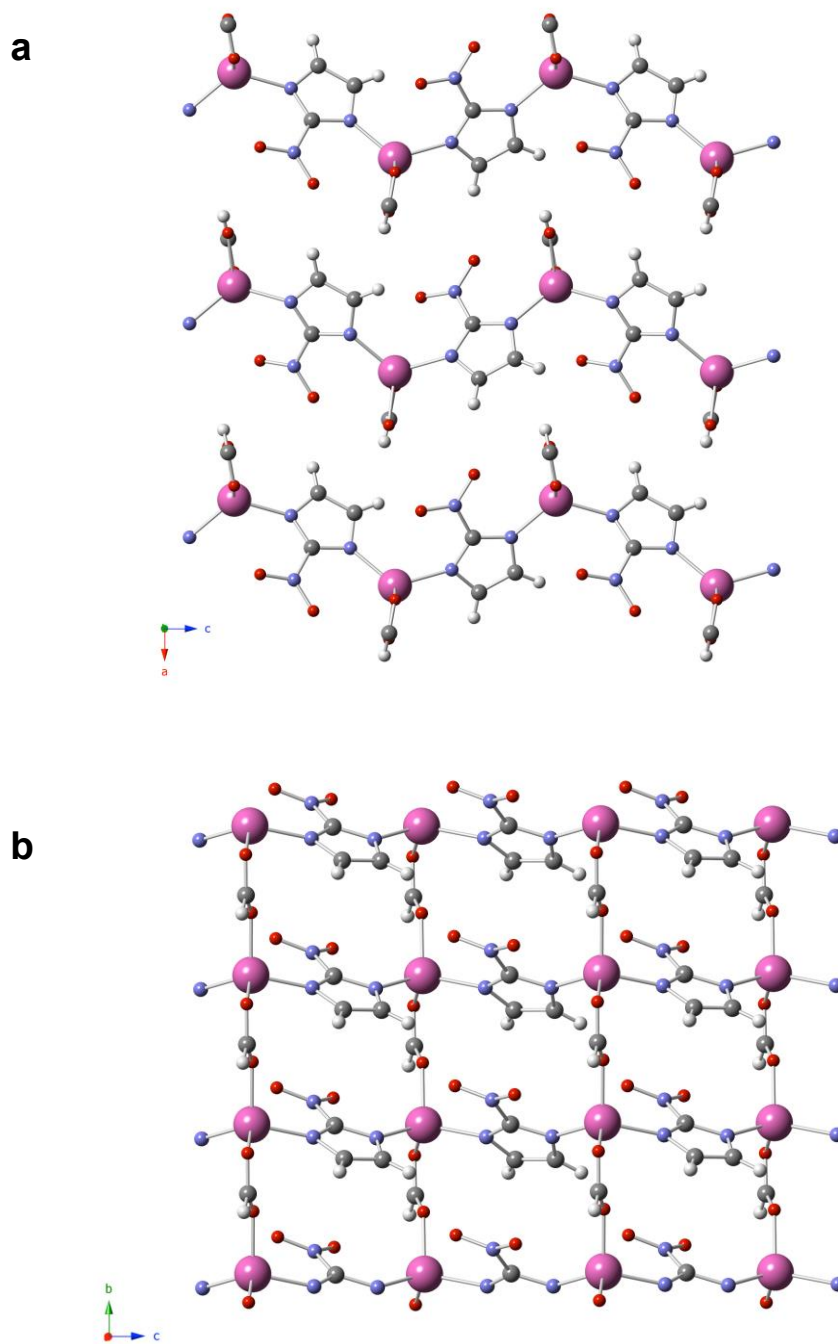


Supplementary Figure S3. Nitric oxide release profiles. NO flux released from NOF-1, NOF-2, [Co(2nIm)₂]_n, 2nIm, mnIm and [Zn(MeIm)₂]_n under sustained illumination at 7.5 mW·cm⁻². Inset: magnification of the low NO flux region, highlighting the absence of NO production from [Zn(MeIm)₂]_n reference material.

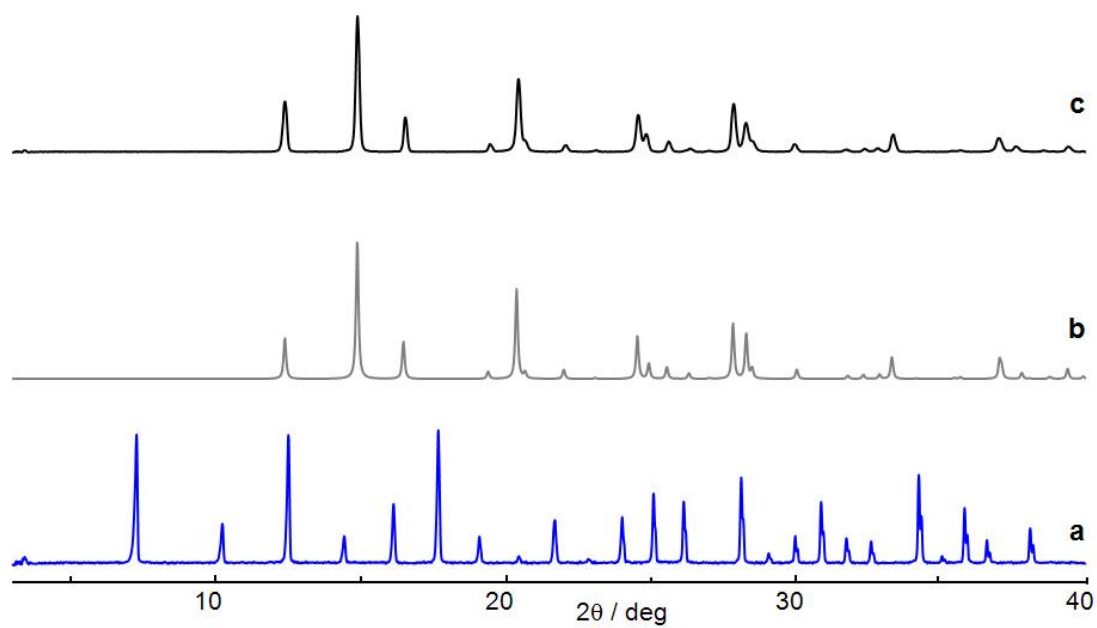
データファイル名 : KSPME.D27
サンプル名 : Sample-He
サンプルID : Rtx5,30.25.25



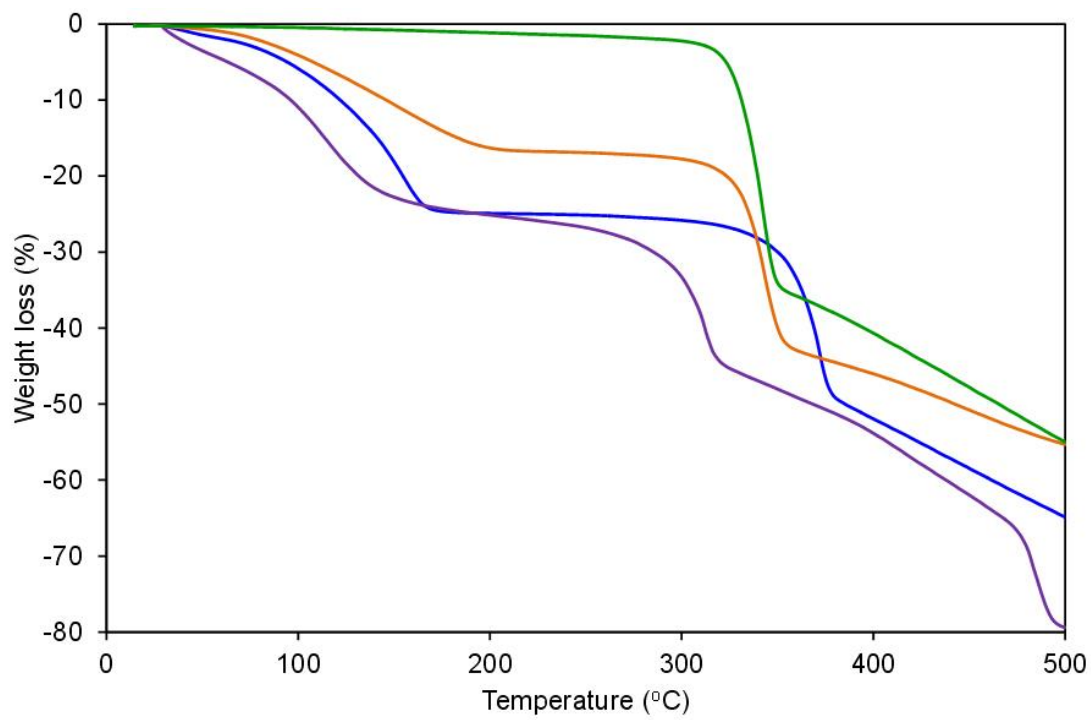
Supplementary Figure S4. GC/MS analysis. The TIC chromatogram was obtained by injecting an aliquot of gas after the irradiation of NOF-1. Nitric oxide trace is highlighted in yellow ($m/z = 30$). Note the absence of NO_2 or N_2O_4 ($m/z = 46$ and 92 respectively), ruling out the occurrence of photolysis of the C- NO_2 bond of 2-nitroimidazole during light irradiation.



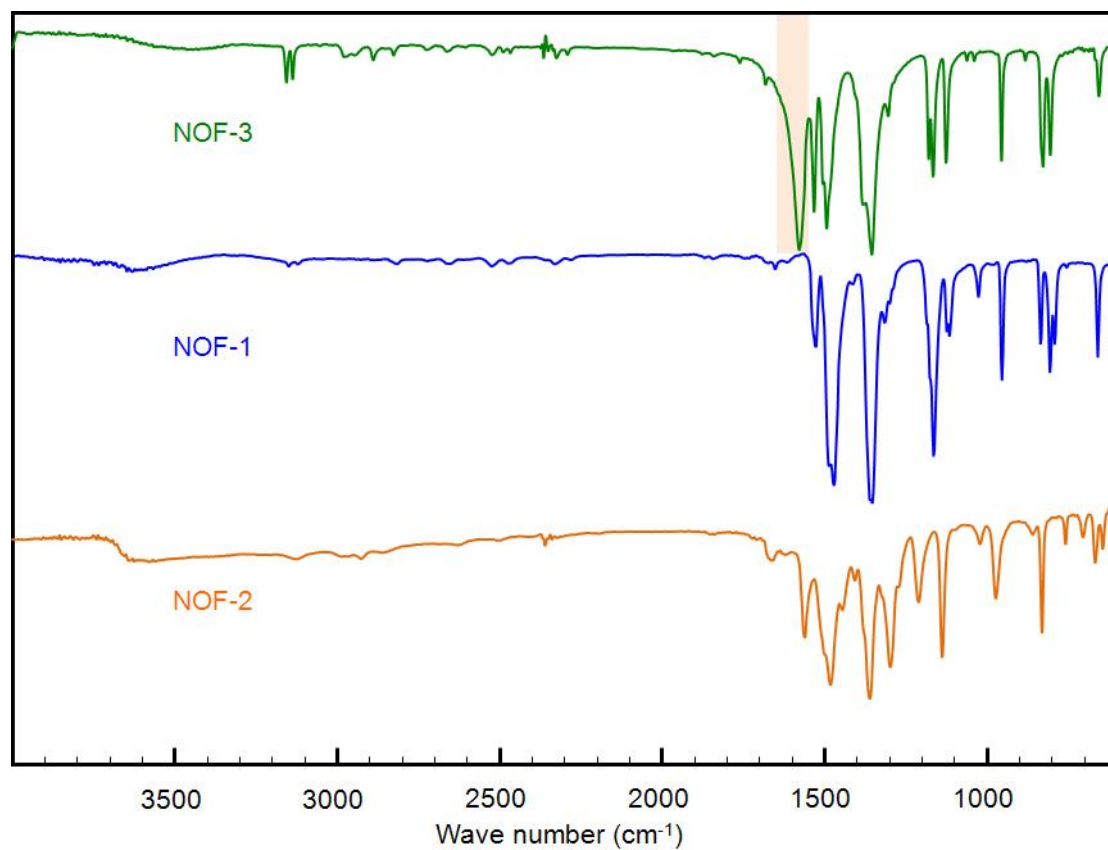
Supplementary Figure S5. Crystallographic representation of the non-porous framework NOF-3. Zinc cations adopt a tetrahedral coordination geometry leading to chains of 2-nitroimidazole (a) which are bridged by formate ligands (b) forming 2-dimensional layers. The formate bridging ligands originate from the hydrolysis reaction of DMF.



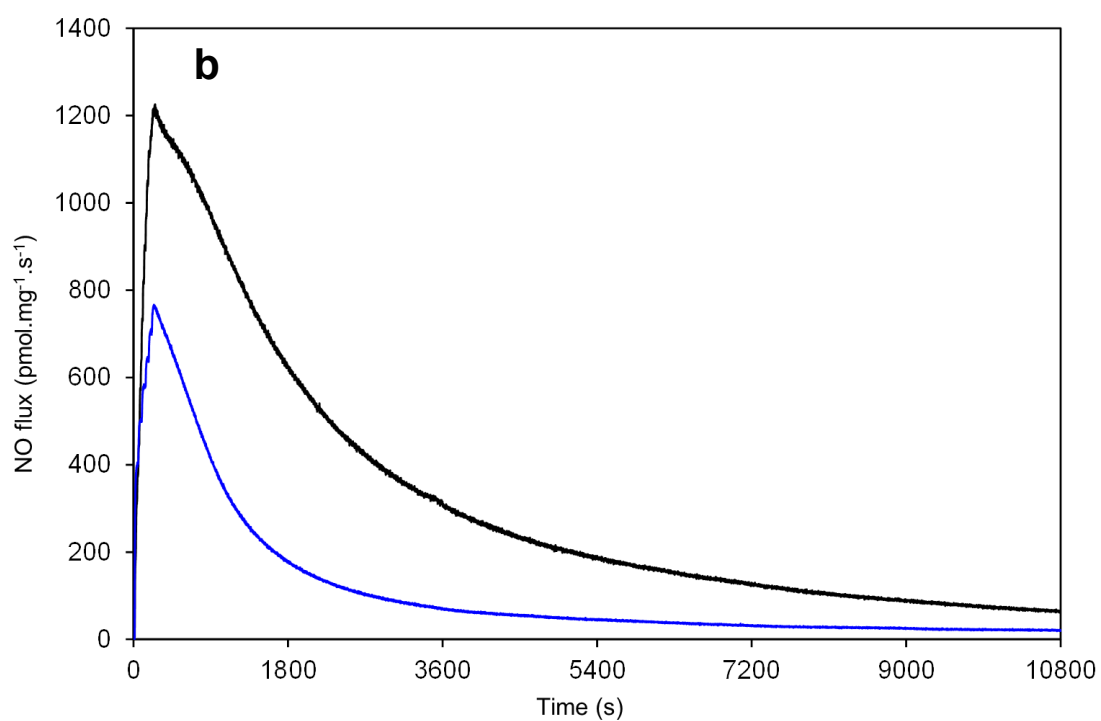
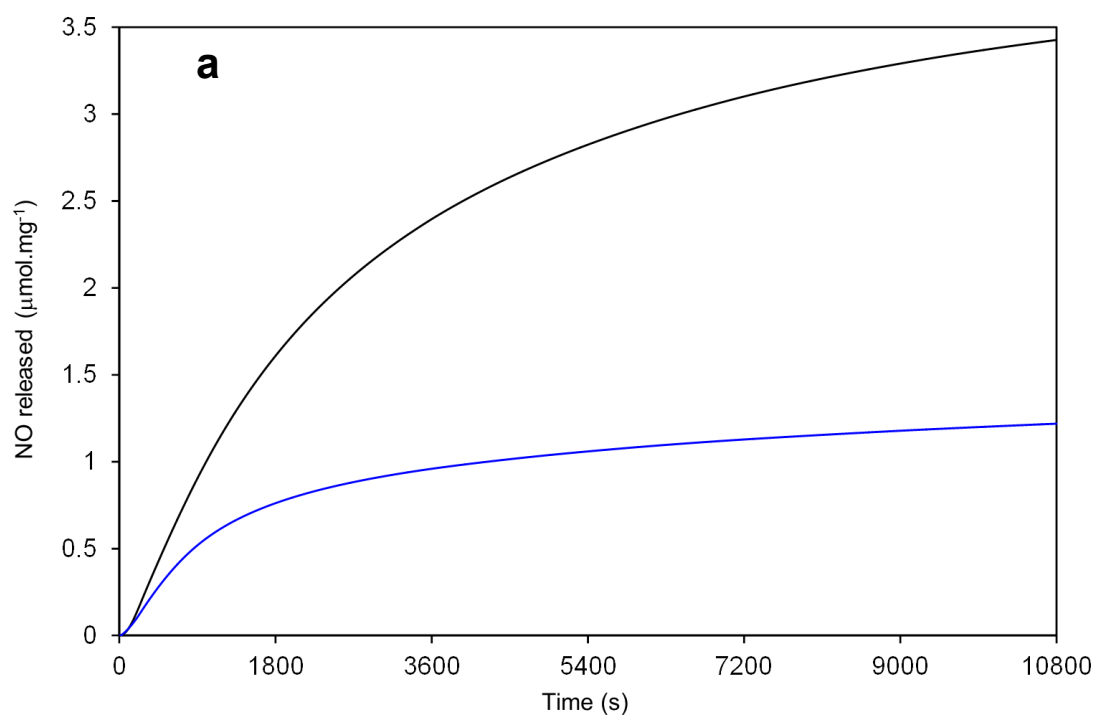
Supplementary Figure S6. Powder X-ray diffraction patterns. The pattern of NOF-1 (**a**) is compared to the simulated diffraction pattern obtained from the SCXRD data form NOF-3 (**b**) and the powder X-ray diffraction patterns of NOF-3 (**c**).



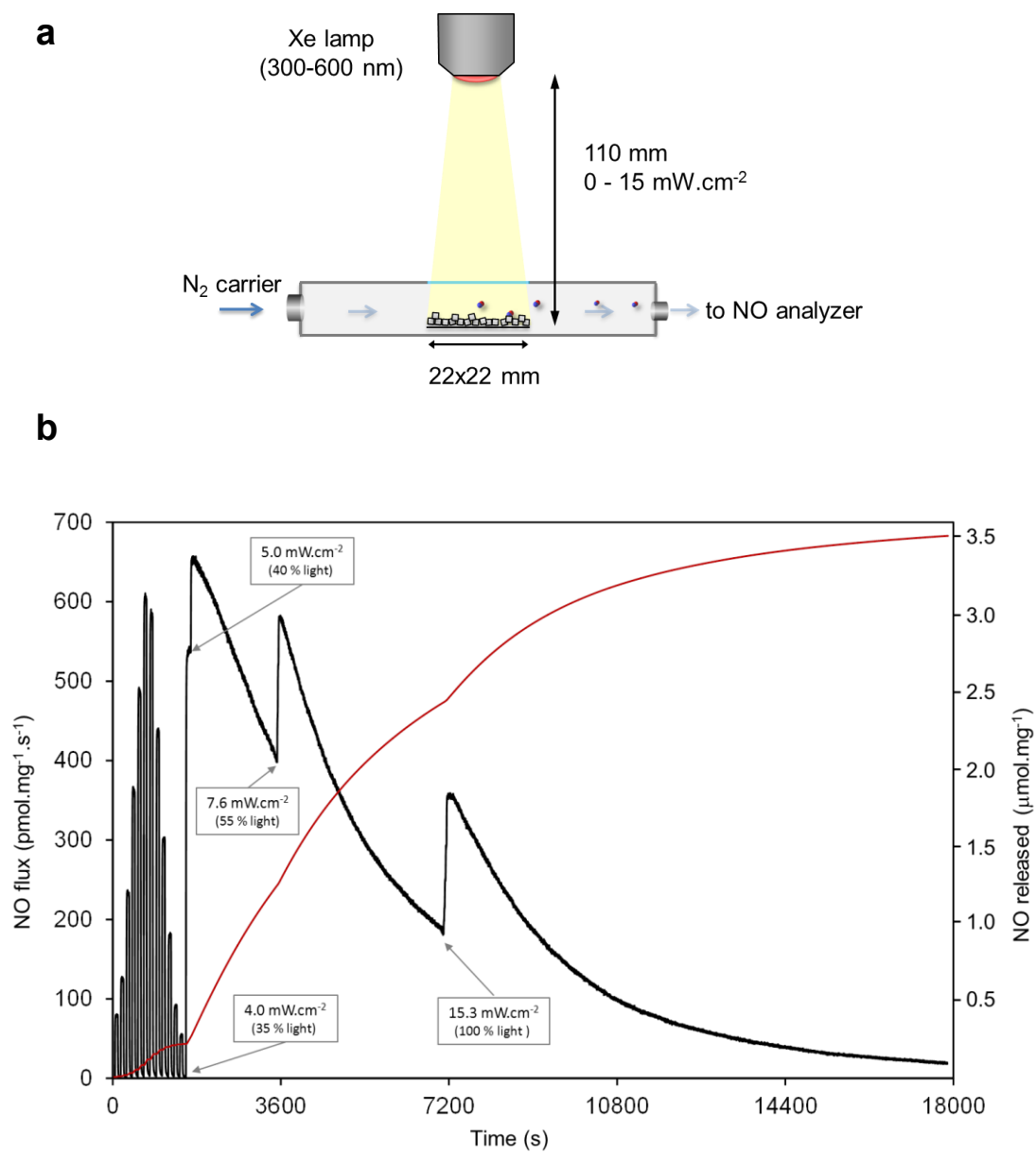
Supplementary Figure S7. Thermogravimetric analysis. TGA curves of as synthesized NOF-1 (blue), NOF-2 (orange), [Co(2nIm)₂]_n (purple) and NOF-3 (green). The absence of significant weight loss until 300°C in NOF-3 is in accordance with its non-porous structure.



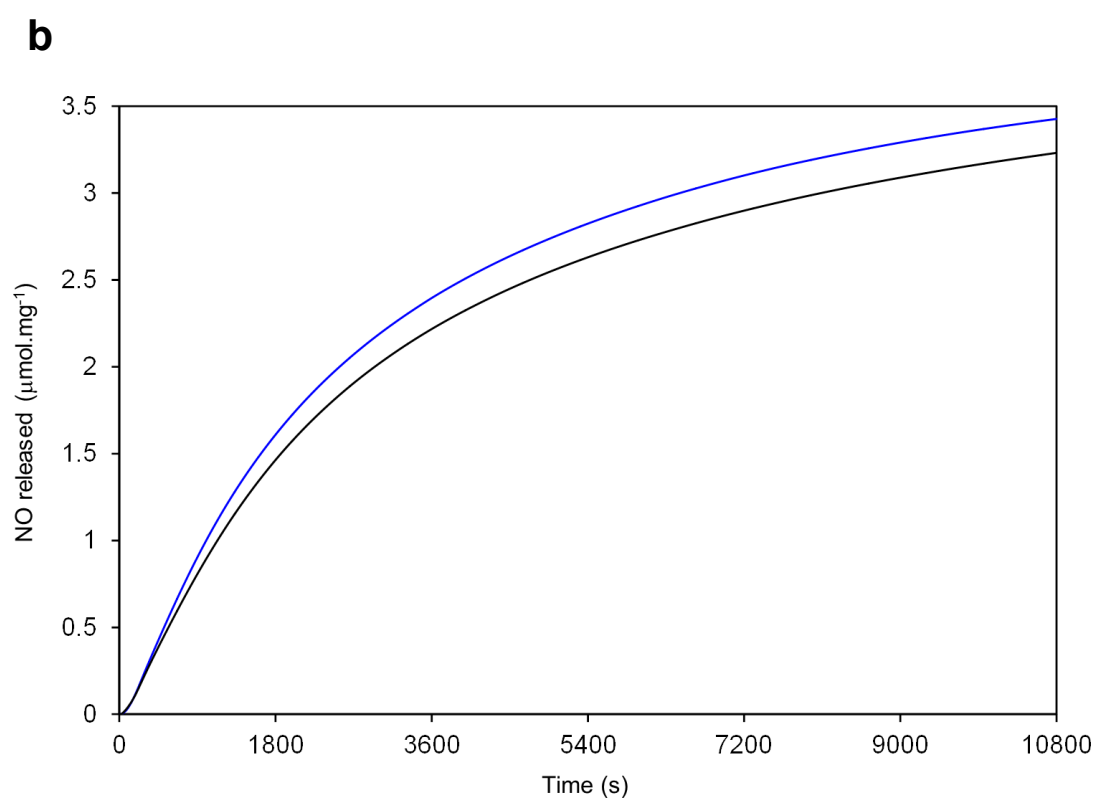
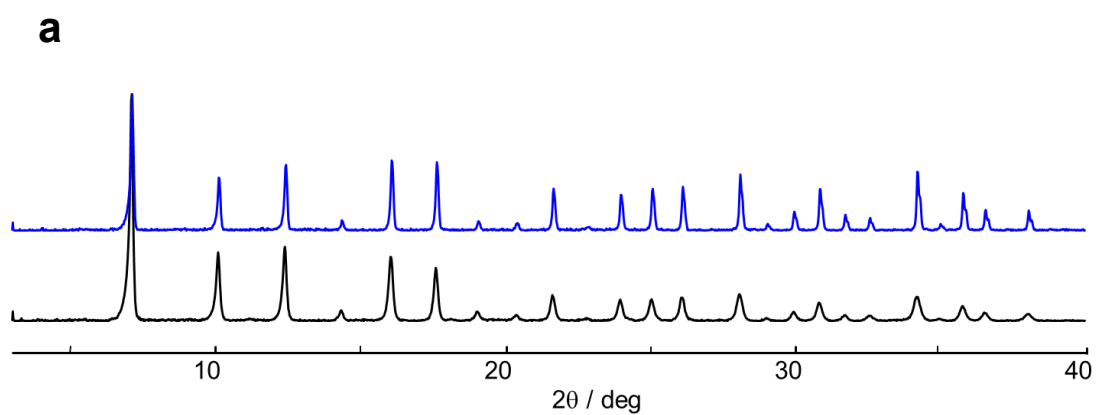
Supplementary Figure S8. Infrared spectroscopy. The presence of additional formate ligands in NOF-3 is evidenced by the appearance of a new intense vibration band at about 1577 cm⁻¹.



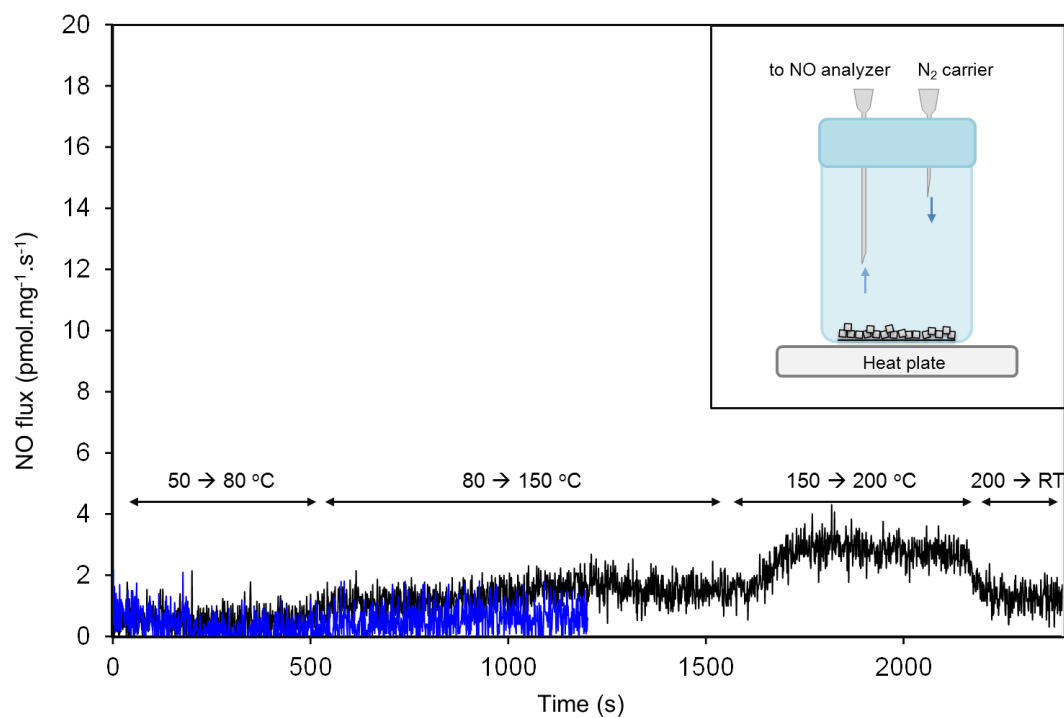
Supplementary Figure S9. Nitric oxide release profiles. Total NO release (a) and NO flux (b) for NOF-1 (blue) and NOF-3 (black) under the same irradiation conditions highlight the more efficient releasing properties of the porous framework NOF-1.



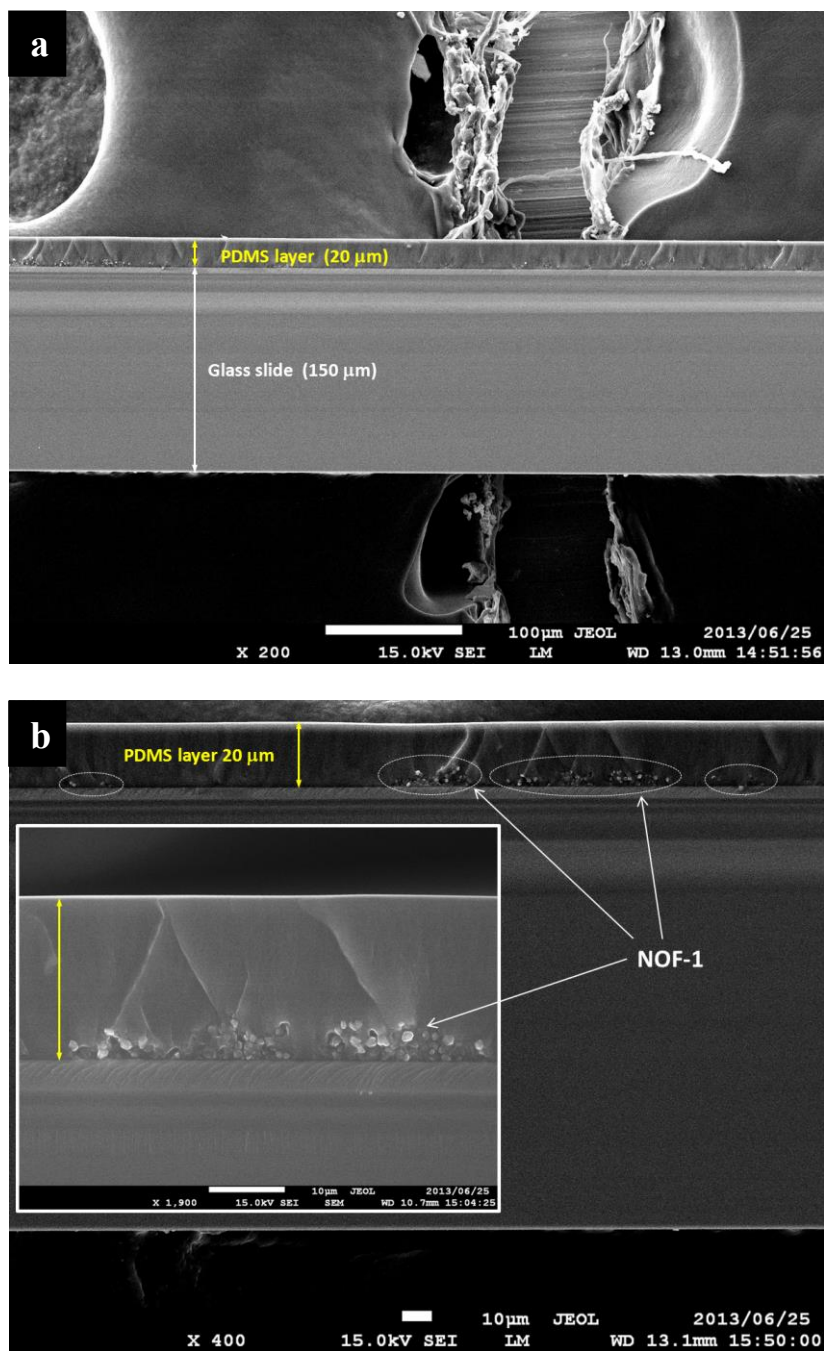
Supplementary Figure S10. Controlled nitric oxide release. Experimental setup for the irradiation experiments (**a**) and NO flux (black) and total NO release (red) for NOF-1 irradiated under light intensities of 0 to 15 mW·cm⁻² (**b**).



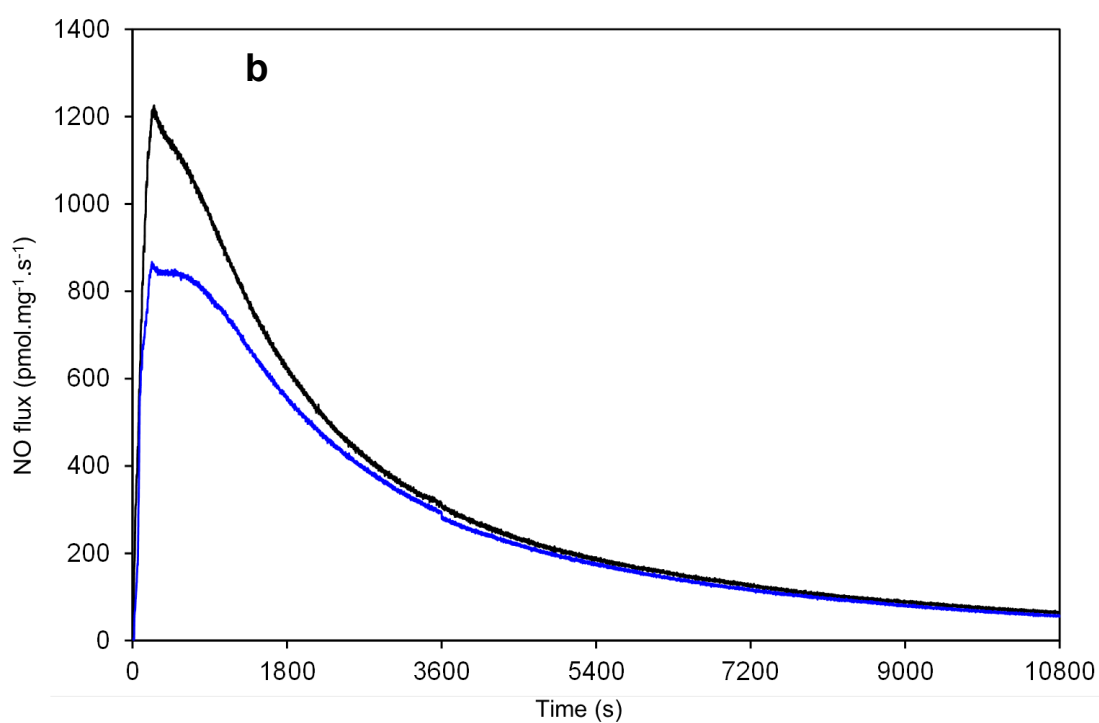
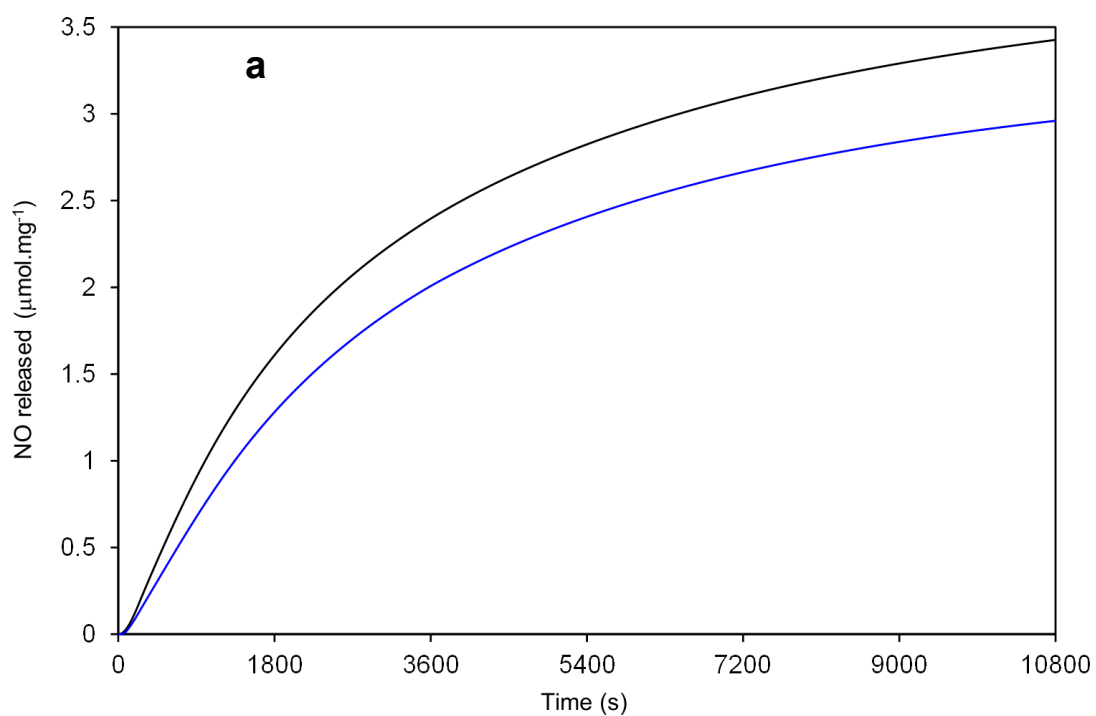
Supplementary Figure S11. Stability of NOF-1. PXRD pattern of freshly prepared NOF-1 (blue) and NOF-1 stored for 8 months in an ambient air-filled vial at room temperature (black) (a). Total NO release of freshly prepared NOF-1 (blue) and after 8 month storage (black) is not significantly altered (b).



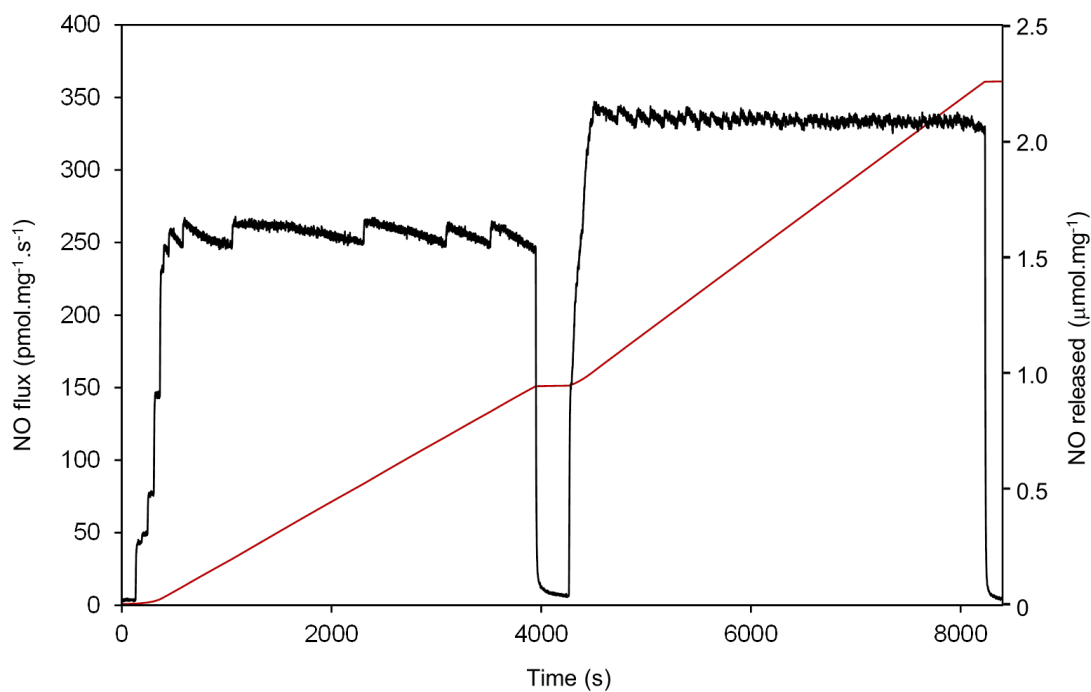
Supplementary Figure S12. Thermal stability of NOF-1. NOF-1 (black) was heated up to 200°C without producing significant amount of NO. The blue line is the raw signal (NO in ppb) for an empty vial heated to 200°C. Inset: scheme of the thermal experiment set up.



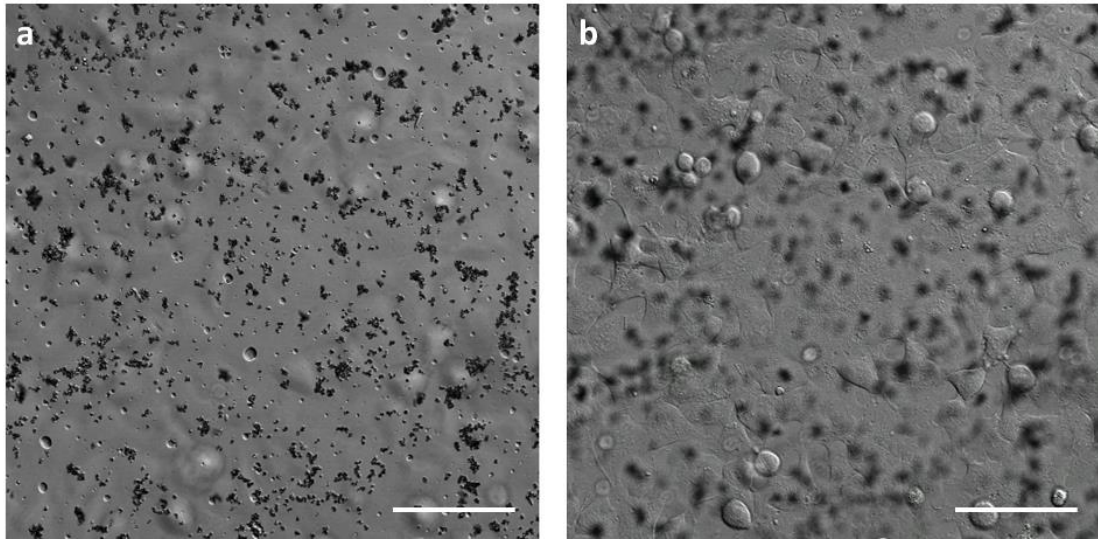
Supplementary Figure S13. Cross-section SEM images of NOF-1/PDMS substrate. The sample was obtained by breaking the NOF-1/PDMS substrate in liquid N_2 and placing the fragments perpendicular to the SEM stage. Observations show a homogeneous PDMS layer (20 μm thickness) throughout the substrate (Scale bars: **a**, 100 μm ; **b** and inset, 10 μm).



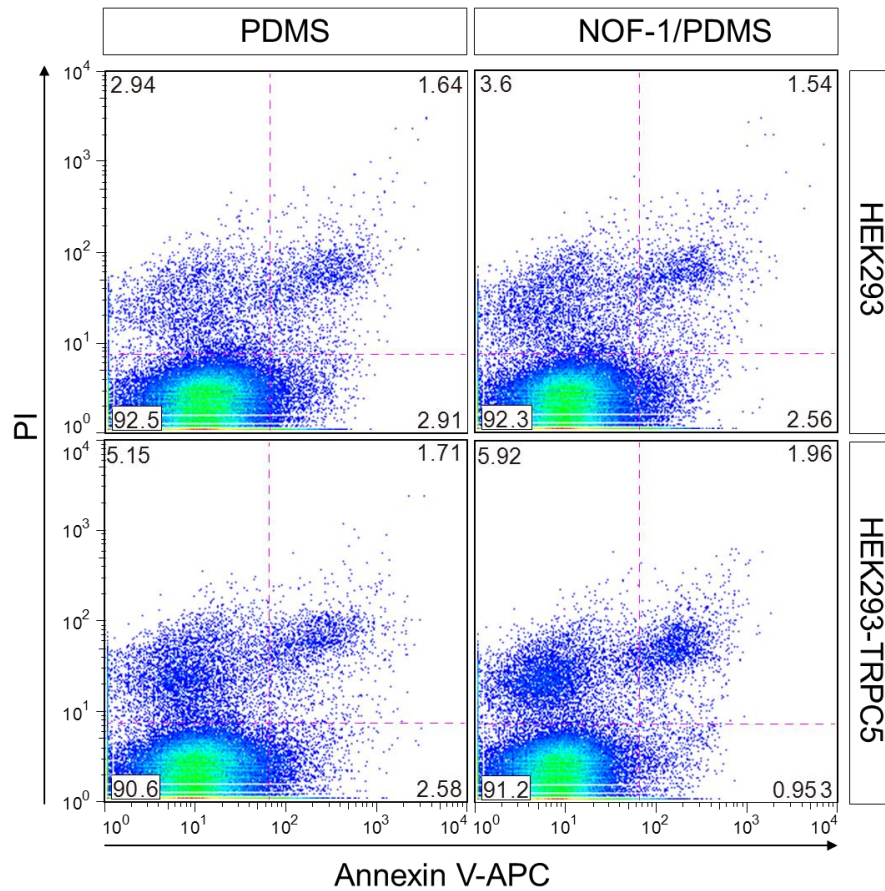
Supplementary Figure S14. Nitric oxide release profiles of NOF-1/PDMS substrate. Total NO release (a) and NO flux (b) for NOF-1 (black) and NOF-1 embedded in a $15 \pm 5 \mu\text{m}$ PDMS layer (blue) under the same irradiation conditions confirm the NO permeability of PDMS. When a neat film of PDMS without any NOF crystals was irradiated, nitric oxide was not detected.



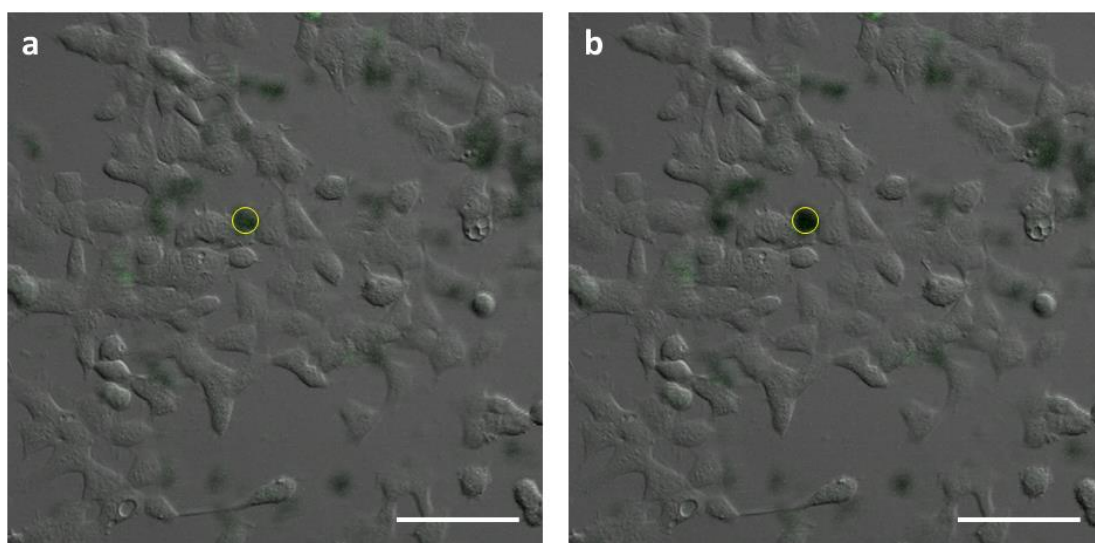
Supplementary Figure S15. Sustained release of nitric oxide. NOF-1/PDMS was irradiated with gradually increasing light intensity in order to provide a sustained and adjustable NO flux for an extended period. The light intensity was adjusted by 1% increments to provide a 250 pmol.mg⁻¹.s⁻¹ NO flux for 1 hour and then a 330 pmol.mg⁻¹.s⁻¹ NO flux for another hour.



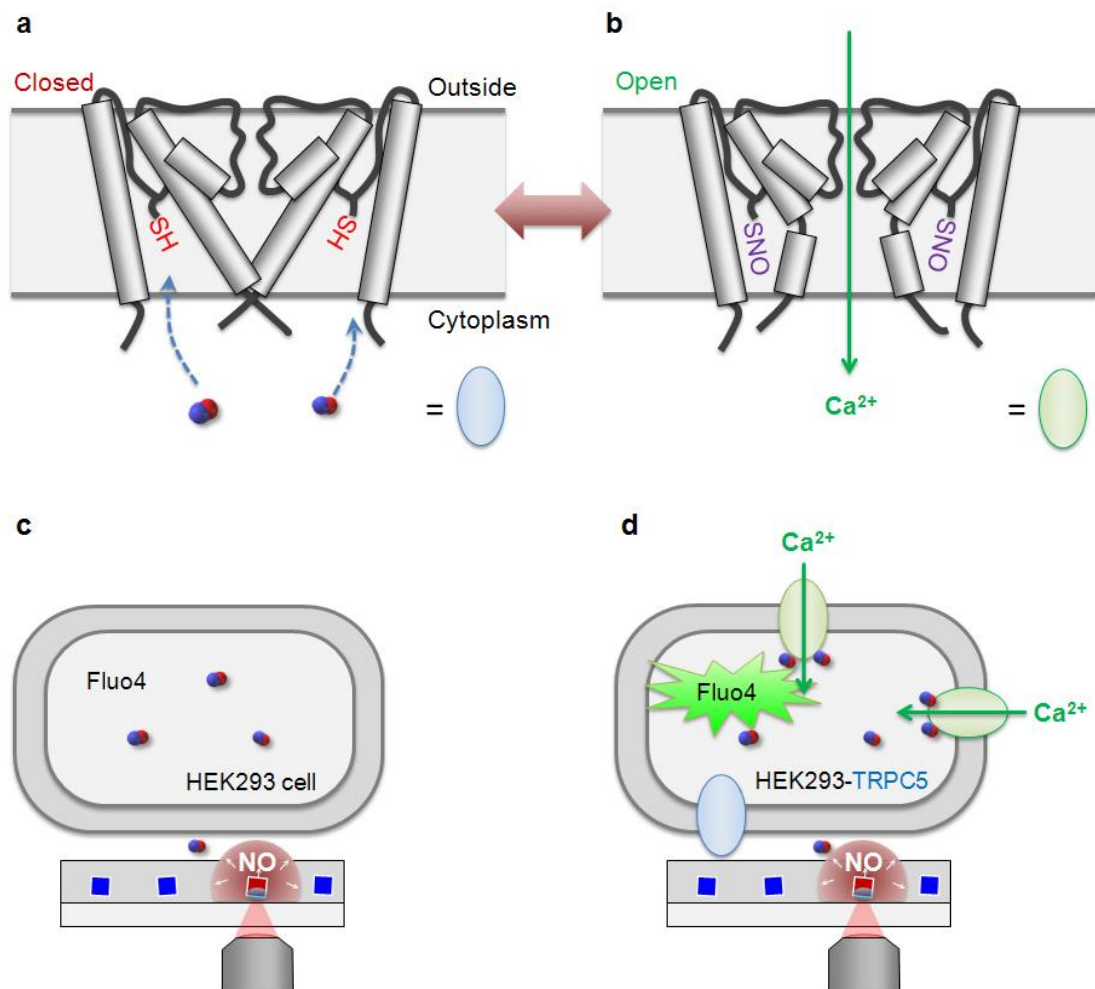
Supplementary Figure S16. Confocal microscopy images. The same substrate was observed at different focal planes (z axis); either on the NOF-1 microcrystals (**a**) or on HEK293 cells (**b**). The distance between the two focal planes is about 15-20 μm . (scale bars: 100 μm)



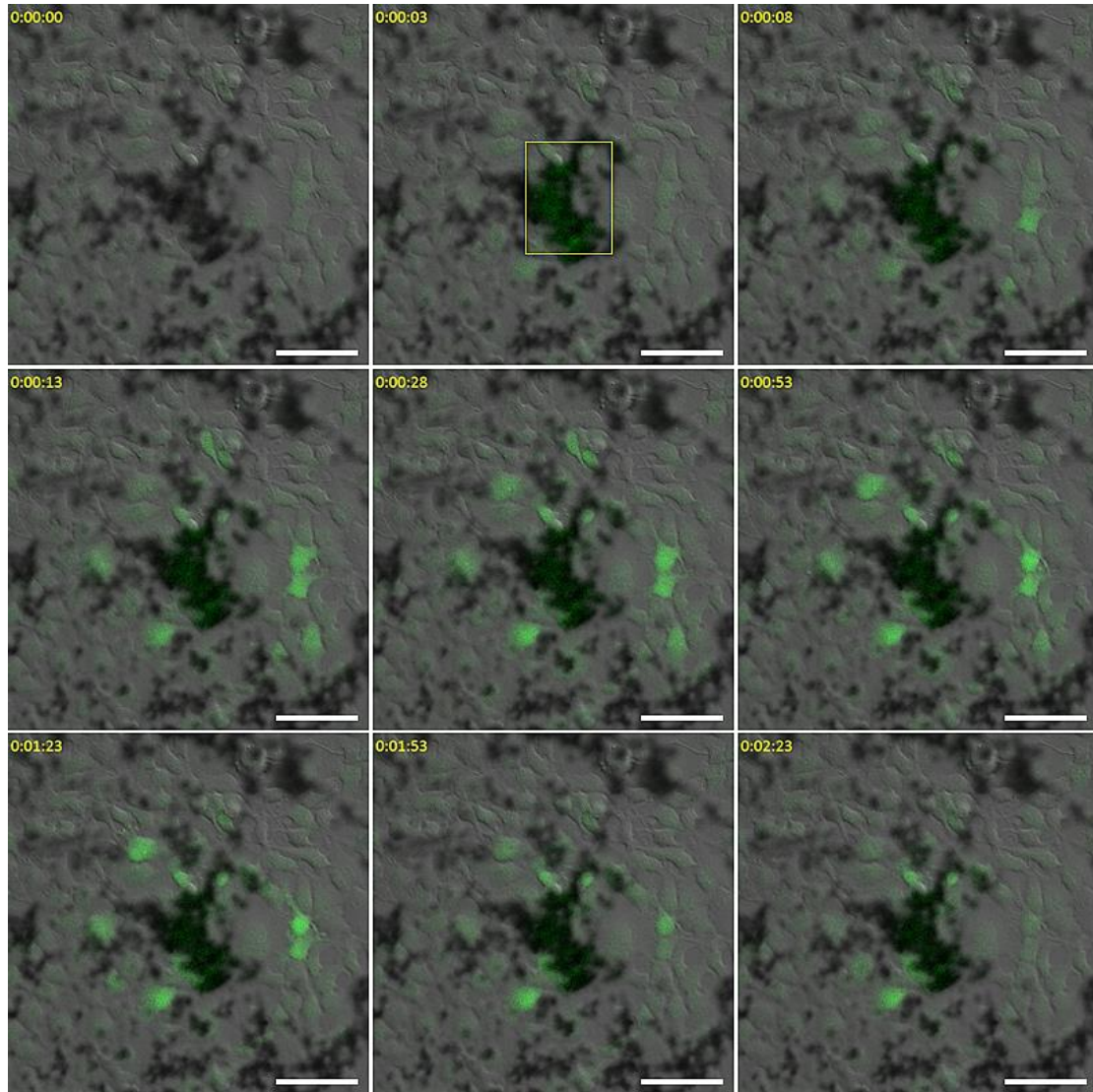
Supplementary Figure S17. Cytotoxicity evaluation. Flow cytometric analysis for early and late apoptotic cells (Annexin V+:PI+ and Annexin V+:PI-, respectively). HEK293 or HEK293-TRPC5 cells were cultured on PDMS or NOF-1/PDMS substrates and then assessed with flow cytometry. Less than 5% of apoptotic cells were observed in all conditions, and NOF-1/PDMS did not present an increased apoptosis induction.



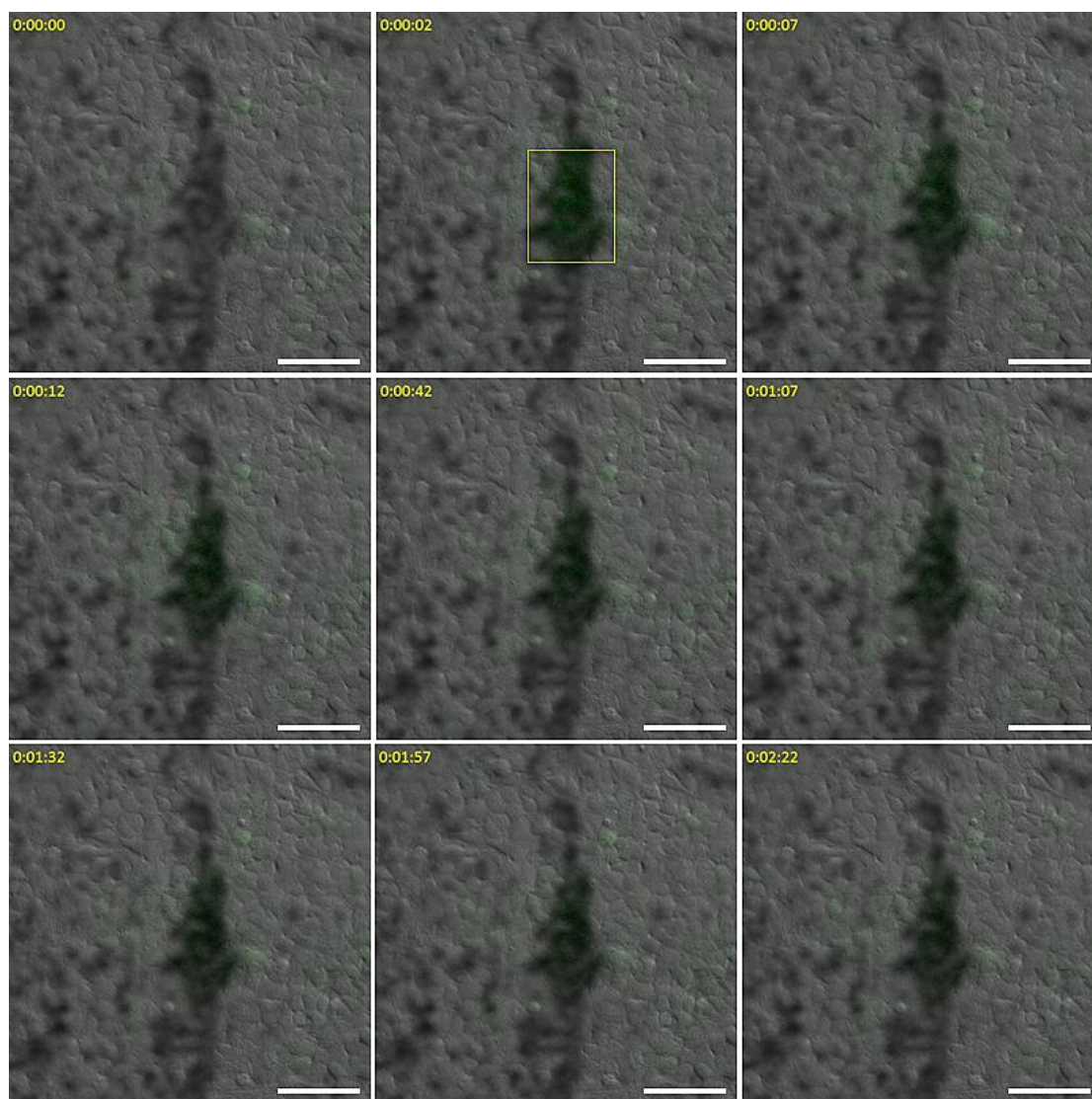
Supplementary Figure S18. Control experiments with analogous framework, $[\text{Zn}(\text{MeIm})_2]_n$. Confocal microscope images of HEK293 cells incubated with DAF-FM before (a) and after (b) two-photon laser irradiation of $[\text{Zn}(\text{MeIm})_2]_n$ /PDMS substrate (region in yellow circle). The absence of fluorescence increase in the cells indicate that NO was not released after photoactivation of $[\text{Zn}(\text{MeIm})_2]_n$ crystals. (scale bars: 100 μm)



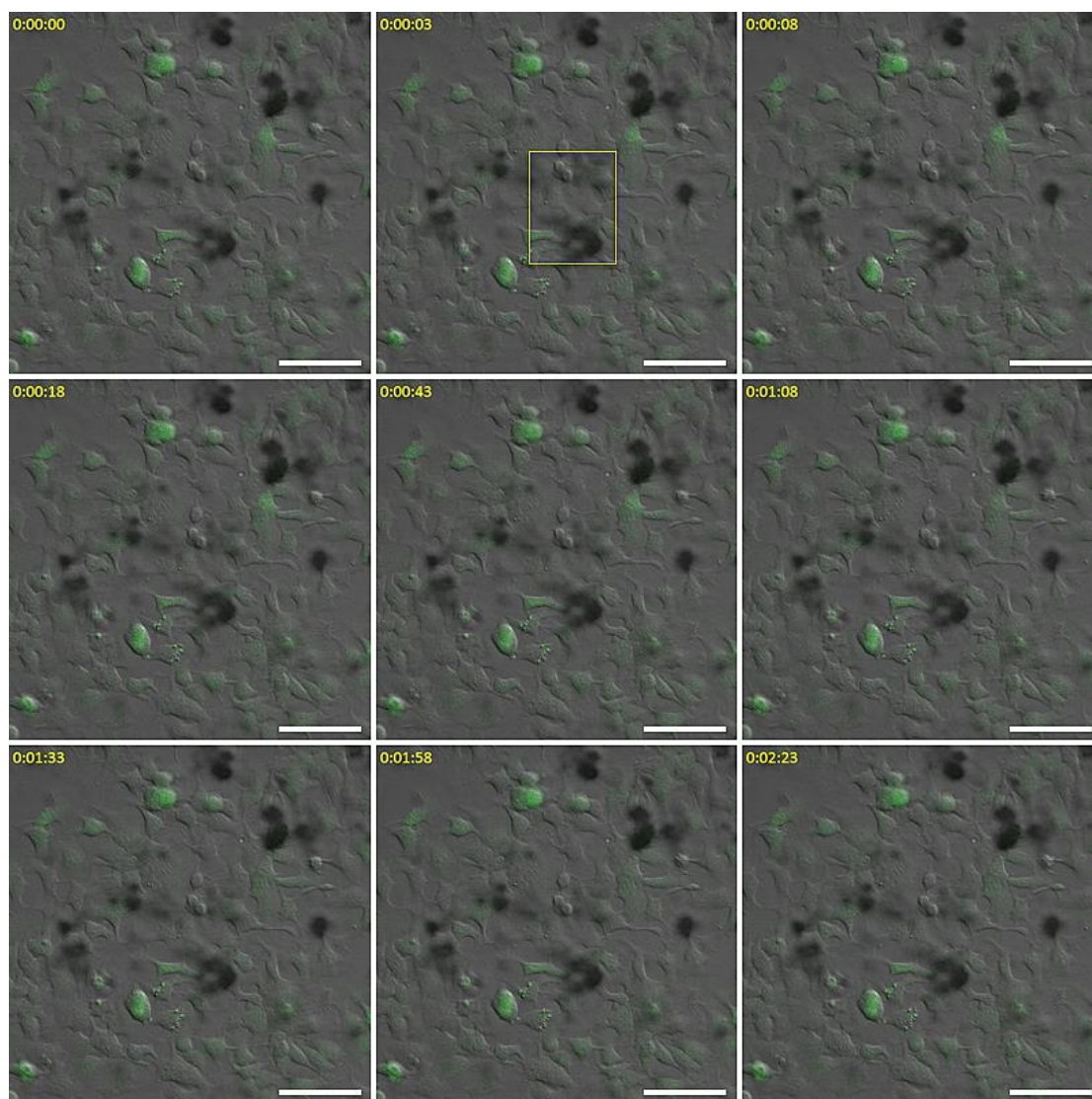
Supplementary Figure S19. Schematic representation of the TRPC5 plasma membrane ion channel. The transition from closed (a) to open (b) forms results from a conformational change induced by *S*-nitrosylation of two cysteine residues located on the cytoplasmic side of the TRPC5 ion channel.⁴⁵ In the control experiment, using native HEK293 cells which are lacking NO-sensitive TRPC5 ion channels, the exogenous NO delivery does not induce any change in intracellular calcium concentration (c). On the other hand, NO uptake in HEK293-TRPC5 cells activates TRPC5 channels and induce a calcium influx from the extracellular media and subsequent increase in Fluo-4 fluorescence (d).



Supplementary Figure S20. Time-course monitoring of calcium levels. Confocal microscope images of NOF-1/PDMS substrate grown with HEK293-TRPC5 cells, showing the evolution of Fluo-4 fluorescence at different timings after the photoactivation of NOF-1 microcrystals (at $t = 3$ s, yellow rectangle area). A clear fluorescence increase is observable few seconds after irradiation. Intensity peaks after about 1 minute and then progressively decreases towards the initial state. (scale bars: 100 μm)



Supplementary Figure S21. Time-course monitoring of calcium levels. Confocal microscope images of NOF-1/PDMS substrate grown with HEK293 cells, showing the evolution of Fluo-4 fluorescence at different timings after the photoactivation of NOF-1 microcrystals (at $t = 2$ s, yellow rectangle area). No change in Fluo-4 fluorescence was observed throughout the experiment. (scale bars: 100 μm)



Supplementary Figure S22. Time-course monitoring of calcium levels. Confocal microscope images of $[\text{Zn}(\text{MeIm})_2]_n/\text{PDMS}$ substrate grown with HEK293-TRPC5 cells, showing the evolution of Fluo-4 fluorescence at different timings after the photoactivation of $[\text{Zn}(\text{MeIm})_2]_n$ microcrystals (at $t = 3$ s, yellow rectangle area). No change in Fluo-4 fluorescence was observed throughout the experiment. (scale bars: 100 μm)

Supplementary Table S1. Crystal data and structure refinement for NOF-1

Empirical formula	C ₆ H ₄ N ₆ O ₄ Zn
Formula weight	289.52
Temperature	135(2) K
Wavelength	0.710474 Å
Crystal system	cubic
Space group	<i>I</i> -43 <i>m</i>
Unit cell dimensions	<i>a</i> = 17.0000(11) Å
Volume	4913.0(6) Å ³
Z	12
Density (calculated)	1.174 Mg/m ³
Absorption coefficient	1.509 mm ⁻¹
<i>F</i> (000)	1728
Crystal size	0.20 x 0.10 x 0.10 mm ³
Theta range for data collection	2.94 to 27.44°.
Index ranges	-18 ≤ <i>h</i> ≤ 22, -22 ≤ <i>k</i> ≤ 22, -22 ≤ <i>l</i> ≤ 17
Reflections collected	19155
Independent reflections	1063 [<i>R</i> (int) = 0.0603]
Completeness to theta = 27.44°	98.5 %
Max. and min. transmission	1.0000 and 0.7990
Refinement method	Full-matrix least-squares on <i>F</i> ²
Data / restraints / parameters	1063 / 0 / 42
Goodness-of-fit on <i>F</i> ²	1.231
Final <i>R</i> indices [<i>I</i> > 2σ(<i>I</i>)]	<i>R</i> ₁ = 0.0746, <i>wR</i> ₂ = 0.1731
<i>R</i> indices (all data)	<i>R</i> ₁ = 0.0747, <i>wR</i> ₂ = 0.1731
Absolute structure parameter	0.08(4)
Largest diff. peak and hole	0.897 and -0.649 e.Å ⁻³

Supplementary Table S2. Crystal data and structure refinement for NOF-2.

Empirical formula	C ₈ H ₈ N ₆ O ₄ Zn
Formula weight	317.57
Temperature	243(2) K
Wavelength	0.710474 Å
Crystal system	trigonal
Space group	<i>R</i> -3 <i>m</i>
Unit cell dimensions	<i>a</i> = 23.132(3) Å <i>c</i> = 15.528(3) Å
Volume	7195(2) Å ³
Z	18
Density (calculated)	1.319 Mg/m ³
Absorption coefficient	1.552 mm ⁻¹
F(000)	2880
Crystal size	0.08 x 0.08 x 0.08 mm ³
Theta range for data collection	2.42 to 30.99°.
Index ranges	-28 ≤ <i>h</i> ≤ 26, -26 ≤ <i>k</i> ≤ 28, -19 ≤ <i>l</i> ≤ 19
Reflections collected	16282
Independent reflections	1689 [<i>R</i> (int) = 0.0388]
Completeness to theta = 26.00°	99.0 %
Max. and min. transmission	1.0000 and 0.0.7378
Refinement method	Full-matrix least-squares on <i>F</i> ²
Data / restraints / parameters	1689 / 0 / 127
Goodness-of-fit on <i>F</i> ²	1.157
Final R indices [<i>I</i> > 2σ(<i>I</i>)]	<i>R</i> ₁ = 0.0577, <i>wR</i> ₂ = 0.1767
R indices (all data)	<i>R</i> ₁ = 0.0589, <i>wR</i> ₂ = 0.1777
Extinction coefficient	0.0031(5)
Largest diff. peak and hole	0.457 and -0.399 e.Å ⁻³

Supplementary Table S3. Crystal data and structure refinement for NOF-3.

Empirical formula	C ₄ H ₃ N ₃ O ₄ Zn
Formula weight	222.46
Temperature	123(2) K
Wavelength	0.710474 Å
Crystal system	orthorhombic
Space group	<i>Pca</i> 2 ₁
Unit cell dimensions	<i>a</i> = 14.2676 (3) Å
	<i>b</i> = 4.5707 (11) Å
	<i>c</i> = 10.7464 (3) Å
Volume	700.8(3) Å ³
Z	4
Density (calculated)	2.108 Mg/m ³
Absorption coefficient	3.48 mm ⁻¹
F(000)	440
Crystal size	0.2 x 0.2 x 0.2 mm ³
Theta range for data collection	4.46 to 27.87°.
Index ranges	-18 ≤ <i>h</i> ≤ 18, -5 ≤ <i>k</i> ≤ 6, -13 ≤ <i>l</i> ≤ 14
Reflections collected	4800
Independent reflections	1509 [<i>R</i> (int) = 0.0257]
Completeness to theta = 27.87°	98.5 %
Max. and min. transmission	1.000 and 0.0.9280
Refinement method	Full-matrix least-squares on <i>F</i> ²
Data / restraints / parameters	1509 / 1 / 109
Goodness-of-fit on <i>F</i> ²	1.075
Final <i>R</i> indices [<i>I</i> > 2σ(<i>I</i>)]	<i>R</i> ₁ = 0.0172, <i>wR</i> ₂ = 0.0465
<i>R</i> indices (all data)	<i>R</i> ₁ = 0.0175, <i>wR</i> ₂ = 0.0468
Absolute structure parameter	0.05(1)
Largest diff. peak and hole	0.328 and -0.444 e.Å ⁻³